Auxiliary Materials for

Independent Confirmation of Global Land Warming without the Use of Station Temperatures

Gilbert P. Compo[1,2*], Prashant D. Sardeshmukh[1,2], Jeffrey S. Whitaker[2], Philip Brohan[3], Philip D. Jones[4,5], Chesley McColl[1,2]

Affiliations:

[1]Cooperative Institute for Research in Environmental Sciences, University of Colorado.

[2]Physical Sciences Division, Earth System Research Laboratory, National Oceanic and Atmospheric Administration.

[3]Met Office Hadley Centre, Exeter, UK.

[4]Climatic Research Unit, University of East Anglia, Norwich, UK.

[5]Center of Excellence for Climate Change Research, Dept of Meteorology, King Abdulaziz University, Jeddah, Saudi Arabia

Introduction

This auxiliary material contains: 1) A description of NOAA National Centers for Environmental Prediction (NCEP) atmosphere/land general circulation model, 2) A description of 20th Century Reanalysis data assimilation system, 3) A description of the data processing of the gridded fields. 4) A description of the Auxiliary figures, 5) Auxiliary figures and captions for Figs. S1 to S3, 6) Auxiliary tables and footnotes for Table S1, S2, and S3, and 6) References for the auxiliary material.

1. Description of National Centers for Environmental Prediction (NCEP) atmosphere/land general circulation model

The short-term forecast ensemble is generated in parallel from 56 9-hour integrations of a state-of-the-art atmospheric and land general circulation model, a 2008 updated version of the

atmospheric and land component of NOAA's National Centers for Environmental Prediction (NCEP) operational Climate Forecast System model [Saha et al., 2006] called the Global Forecast System (GFS). The AMIP20C ensemble is generated from 56 138-year integrations of the GFS. Briefly, the atmospheric model component of the GFS used here has a spatial resolution of nearly 200-km on an irregular Gaussian grid in the horizontal (corresponding to a spherical harmonic representation of model fields truncated at total wavenumber 62, T62). In the vertical, we use finite differencing of 28 hybrid sigma-pressure levels [Juang, 2005]. The model state includes a comprehensive suite of atmospheric fields (e.g., surface pressure, horizontal winds and vertical motion, temperature, and humidity). The model has a complete suite of physical parameterizations representing the exchange of heat, momentum, and moisture [Kanamitsu et al., 1991] with most updates detailed in Moorthi et al. [2001]. Additional updates to these parameterizations are described in Saha et al. [2006] and Compo et al. [2011] and include revised solar radiation transfer, boundary layer vertical diffusion, cumulus convection, and gravity wave drag parameterizations. In addition, cloud liquid water is a prognostic quantity with a simple cloud microphysics parameterization. The radiation interacts with a fractional cloud cover that is diagnostically determined by the predicted cloud liquid water. A prognostic ozone parameterization is also included in the GFS based on parts of the US Naval Research Laboratory's CHEM2D Ozone Photochemistry Parameterization (CHEM2D-OPP) [McCormack et al., 2006]. It includes terms representing gas phase net production and loss and a dependency on the ozone mixing ratio itself. The 2008 version of the GFS model used also includes the radiative effects of historical time-varying CO_2 concentrations, volcanic aerosol and solar variations. Monthly estimates of CO_2 concentration on a 15° latitude by longitude grid are used from 1956 to 2010 and half-yearly globally-averaged estimates are used prior. Annual estimates

of solar variations are used from 1944 to 2010, and a repeating 11 year solar cycle is used prior. Monthly estimates of volcanic aerosols are used. The model contains a complex representation of land processes through coupling with the 4-layer Noah land model [Ek et al., 2003]. The specified boundary conditions needed to run the model in atmosphere/land mode are taken from the time-evolving sea surface temperature and sea ice fields of the HadISST1.1 dataset obtained courtesy of the Met Office Hadley Centre [Rayner et al., 2003]. The success of the AMIP20C (Table S2, Fig. S2, S3) and of other SST-forced simulations [e.g., Compo and Sardeshmukh, 2009; Hoerling et al., 2008] indicates that the adjustment procedures for the SST observations are appropriate, at least in so far as they relate to determining TL_{2m} from the simulations. Note that these adjustments tend to make the SSTs in the first half of the 20th century warmer than the original, uncorrected observations [Rayner et al., 2003]. It is easy to hypothesize that if we had used unadjusted SSTs, even more warming of the land temperatures would have been found in AMIP20C, and potentially in 20CR, over the period 1901 to 2010.

2. Description of 20th Century Reanalysis Data assimilation System

The 20th Century Reanalysis (20CR) is a physically-based state-of-the-art data assimilation system that generates a six-hourly estimate of the 3 dimensional state of the atmosphere and the uncertainty in that state using only CO_2, solar and volcanic radiative forcing agents [Compo et al., 2011]; monthly-averaged sea surface temperature (SST) and sea ice concentration fields (both from the HadISST1.1 of Rayner et al. [2003]); and hourly and synoptic barometric pressure observations (from the International Surface Pressure Databank [Compo et al., 2011]). The 20CR is based on an Ensemble Kalman Filter technique [Whitaker and Hamill, 2002]. The atmospheric state is estimated ("analyzed") every six hours from a weighted combination of available pressure observations and an ensemble of 56 nine-hour forecasts made from the previous

79 estimated state using a NOAA atmosphere/land general circulation model (AGCM, see auxiliary
80 material Section 1) developed at NCEP. This weighting, the Kalman gain, is determined from the
81 covariance matrix of the forecast ensemble [Whitaker and Hamill, 2002]. The Kalman gain
82 varies from analysis to analysis depending on the physical features of the flow, such that when
83 the ensemble spread of the forecasts is large in regions of rapidly growing uncertainty, e.g.,
84 during a developing low-pressure weather system, more weight is given to the observations and
85 less to the forecasts. It also varies such that more weight is given to each observation when the
86 observations are sparse. Sampling and model errors prevent the ensemble-estimated Kalman gain
87 from being optimal and can lead to filter divergence [e.g., Anderson and Anderson, 1999;
88 Whitaker and Hamill, 2002]. Two methods are used to account for this: covariance inflation
89 [Anderson and Anderson, 1999] and distance-dependent covariance localization [Houtekamer
90 and Mitchell, 2001; Hamill et al., 2001]. Covariance inflation attempts to correct for sampling
91 error and serves as a parameterization of model error, assuming that the model error covariance
92 is in the space of the 56 ensemble states. In the 20CR, covariance localization coefficients are set
93 to 4 scale heights in the vertical (about 18 hPa) and 4000 km in the horizontal. They are constant
94 throughout the reanalysis period [Compo et al. 2011]. The coefficients for covariance inflation
95 change at stated times throughout the interval. Less inflation is needed during times and in
96 regions where the observations are sparse, while more is needed as the pressure observations
97 become denser in the 2nd half of the 20th century. Inflation coefficients have a maximum 12% in
98 the Northern Hemisphere starting in 1921 and 7% in the Tropics and Southern Hemisphere
99 starting in 1952. The coefficients remain constant starting in 1952 [See Table I, Compo et al.
100 2011]. The year 1952 thus forms an ideal starting point for computing trends from 20CR and is

101 therefore used as the initial year for some of the calculations in Fig. 2, 3, Table S2, Table S3, and
102 Fig. S3.

103

104 Each state estimate in 20CR includes fields of surface pressure and 3 dimensional winds,
105 temperature, humidity, cloud liquid water, and ozone at 28 vertical levels throughout the
106 troposphere and stratosphere around the globe on an approximately 2 degree latitude by 2 degree
107 longitude grid [Compo et al., 2011]. In addition to the variables included in the state estimate, the
108 forecast also includes variables on the global grid such as fluxes of heat, momentum, radiation
109 and moisture [Compo et al., 2011].

110

111 **3. Data Processing**

112 To facilitate the intercomparison of 20CR with the available TL_{2m} observational data sets, we
113 have spatially interpolated each monthly field of the datasets 20CR, CRU_TS3.10,
114 GISTEMP250 and GISTEMP1200, JMATEMP, and UDELv3.01 to a 1.5 degree latitude by 1.5
115 degree longitude grid using natural neighbor interpolation to determine the land-average for
116 90°N-60°S (Fig. 1, Table S2) and 60°N-60°S (Fig. S1, Table S3). MLOSTv3.5.2 was
117 interpolated only for the 90°N-60°S comparison in Fig. 1 and Table S2. The CRU_TS3.10 was
118 used to define a common set of land grid points. The CRUTEM3 uncertainty model [Brohan et
119 al., 2006] was used to construct the land averages and associated uncertainty estimates for
120 CRUTEM3 and CRUTEM4 for 90°N to 60°S (Table S2) and 60°N to 60°S (Fig. S1, Table S3).
121 NOAA provides the land-average and associated uncertainty for MLOSTv3.5.2 for the region
122 60°N-60°S (Table S3). The fractional land/sea mask of MLOST was used for the time series

123 calculations for MLOST and JMATEMP as both are ocean and land blended analyses.
124 Anomalies in a dataset were defined as the difference of each monthly grid point value from the
125 1981 to 2010 monthly average for that dataset grid point. Least squares linear trends are
126 computed on the native grid of each dataset and then interpolated to the 1.5 degree latitude by
127 1.5 degree longitude grid for computation of the comparison statistics between trend maps in
128 Table S2 and Fig. 3.

129

130 **4. Description of Auxiliary Figures**

131

132 To compare the actual and expected mean square differences, an F-test is used. The required
133 degrees of freedom are derived by accounting for the auto-correlation [Livezey and Chen, 1983]
134 in the difference series of 20CR TL_{2m} minus the station temperature dataset TL_{2m} (Fig. S1, right
135 panels). The combined 95% uncertainty is formed by adding the error variances for each annual
136 anomaly from the 20CR ensemble and the respective temperature dataset, taking the square root,
137 and multiplying by +/- 1.96, assuming that the errors are Normally distributed. While the overall
138 correspondence is high (Table S3), low-frequency variability in the differences is apparent (Fig.
139 S1). Such low-frequency variability, rather than a trend, indicates that these differences do not
140 arise from an "urban warming" effect that remains in the land station datasets.

141

142 Taking the mean of the square of the differences shown in the right panels of Fig. S1 forms the
143 Mean Squared Difference in Table S3. Dividing the combined 95% uncertainty by 1.96 and
144 taking the time-mean of the squared quantity forms the Expected Mean Squared Difference
145 (Table S3). If the errors are random, the expected value of the variance of analysis minus

146 independent observation residuals in an optimal data assimilation system is simply the ensemble
147 variance in observation space plus the observation error variance [Kalnay, 2003]. As is visible
148 from Fig. S1, the differences depart from zero more frequently than expected, except for the
149 MLOST dataset after 1952. Difference series do not show a clear trend that could be interpreted
150 as a residual "urban warming" affecting the gridded temperature datasets (Fig. S1). It also
151 appears that the differences and error estimates are consistent for the period before World War II
152 (pre-1941) for the datasets shown in Fig. S1.
153
154 The local TL_{2m} trend patterns for the 1901-2010 period (Fig. S2) and for the 1952-2010 period
155 (Fig. S3) were used in the calculation of the comparison statistics in Table S2 and Fig. 3 and are
156 shown here for completeness. It is apparent that each dataset has some regional deviations not
157 reflected in other datasets, such as differences over the Midwestern US and in the vicinity of
158 Brazil and Argentina. We note that there is a greater degree of spatial smoothness in the
159 analyses of GISTEMP and MLOST compared to the other station temperature datasets. This
160 arises from the relatively large smoothing box sizes in the GISTEMP analyses (1200 km and 250
161 km) and from the use of empirical orthogonal teleconnections in the MLOST reconstruction.

162 **5. Auxiliary figures and captions**

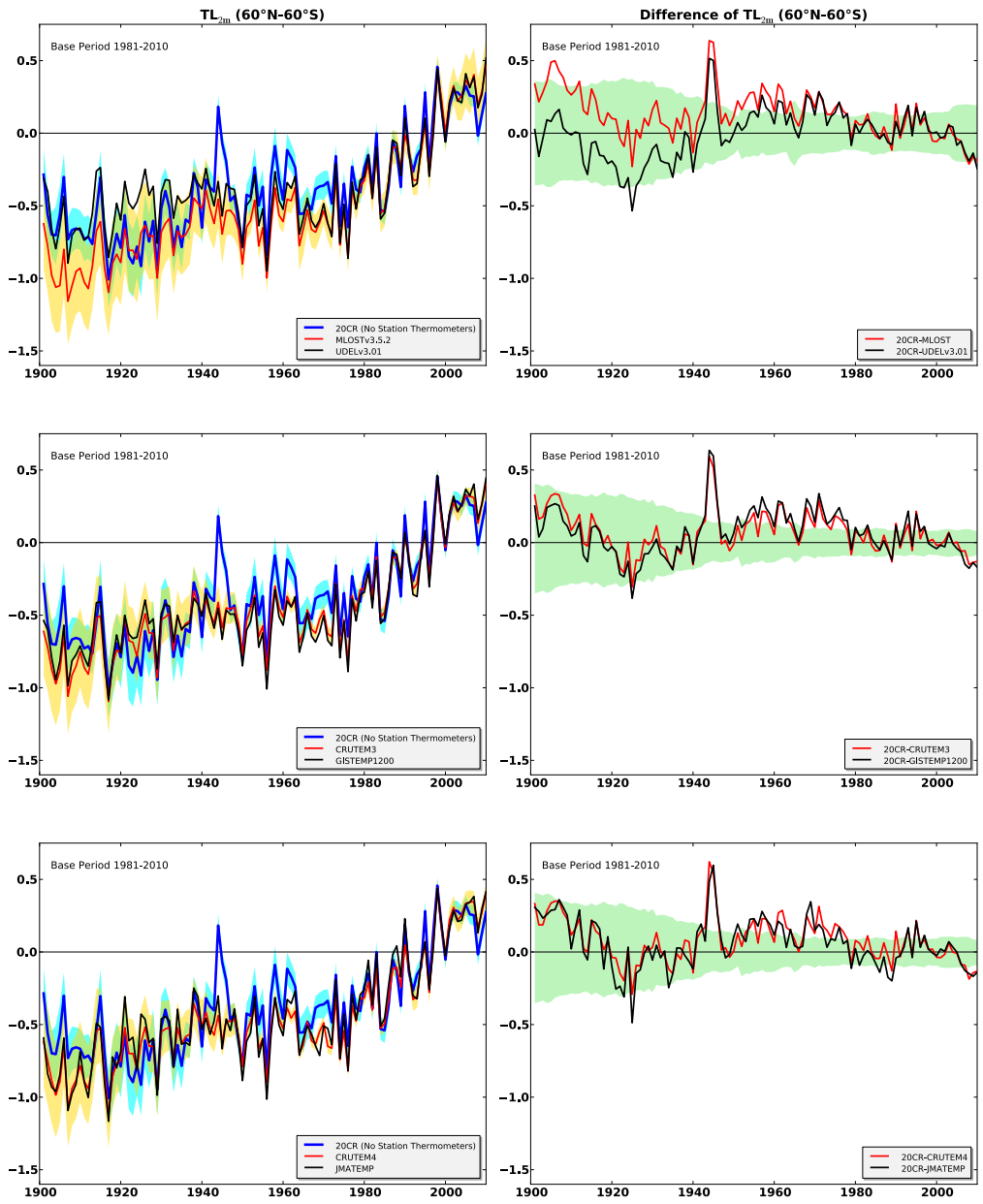

Fig. S1. Comparison between time series of annually-averaged near-global (60°N-60°S) TL_{2m} anomalies from (left panels) 20CR and station temperature based estimates and (right panels) comparing their differences. [Left panels] Compared are anomaly series from 20CR (blue curve) and [top left] MLOSTv3.5.2 (red curve) and UDELv3.01 (black curve); [middle left] CRUTEM3 (red curve) and GISTEMP1200 (black curve); and [bottom left] CRUTEM4 (red curve) and JMATEMP (black curve). 95% uncertainty ranges are shown for [top to bottom],

170 respectively, MLOSTv3.5.2, CRUTEM3, and CRUTEM4 (yellow fill) and 20CR (blue fill) and
171 their overlap (green fill). Right panels show the difference of each dataset from 20CR and the
172 combined 95% uncertainty.
173

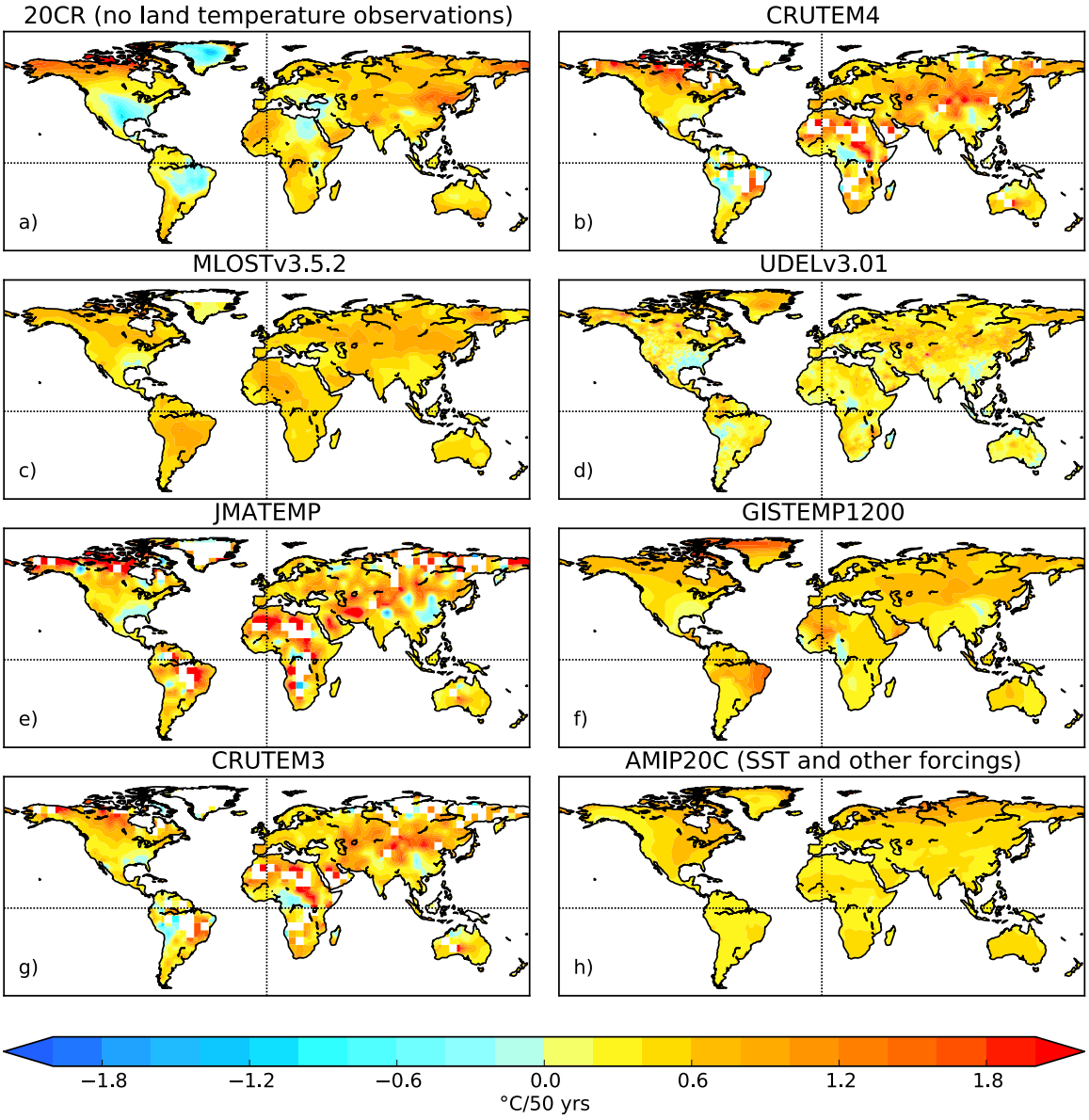

174
175 **Fig. S2.** Spatial comparison of TL_{2m} trends between 20CR and the station-temperature datasets
176 listed in Table S2 over the 1901-2010 period. The 20CR trend map is reproduced from Fig. 2b
177 for ease of comparison. Trends are shown as °C change per 50 years.

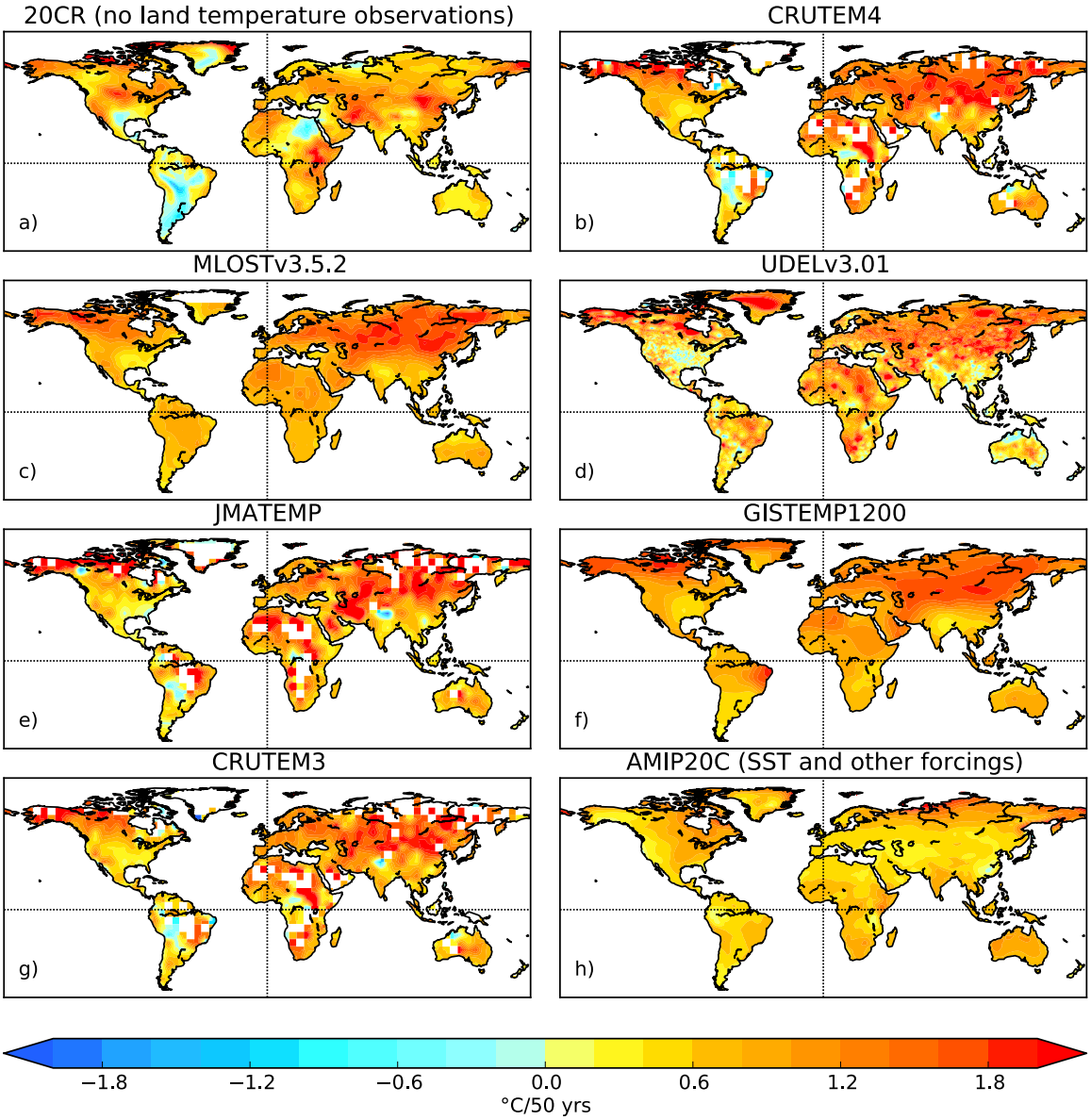

178
179 **Fig. S3.** As in Fig. S2, but local linear trends are computed over 1952-2010 periods. The 20CR
180 map is reproduced from Fig. 2d for ease of comparison.

181

182

183

184

185

5. Auxiliary Tables and footnotes

Table S1. Publicly available sources for each dataset[a].

20CR	http://go.usa.gov/XTd http://rda.ucar.edu/datasets/ds131.1/ http://portal.nersc.gov/project/20C_Reanalysis (+)
CRUTEM3	http://www.metoffice.gov.uk/hadobs/crutem3, http://www.cru.uea.ac.uk/cru/data/temperature/ http://www.esrl.noaa.gov/psd/data/gridded/data.crutem3.html (+)
CRUTEM4	http://www.metoffice.gov.uk/hadobs/crutem4 http://www.cru.uea.ac.uk/cru/data/temperature/ http://www.esrl.noaa.gov/psd/data/gridded/data.crutem4.html (+)
CRU_TS3.10	http://badc.nerc.ac.uk/view/badc.nerc.ac.uk__ATOM__ACTIVITY_fe67d66a-5b02-11e0-88c9-00e081470265 (+)
GISTEMP 250 km smoothing GISTEMP 1200 km smoothing	http://data.giss.nasa.gov/gistemp/ http://www.esrl.noaa.gov/psd/data/gridded/data.gisstemp.html (+)
JMATEMP	http://ds.data.jma.go.jp/tcc/tcc/products/gwp/gwp.html (+)
MLOSTv3.5.2.201211	http://www.ncdc.noaa.gov/ersst/merge.php ftp://ftp.ncdc.noaa.gov/pub/data/mlost/operational/products/ (+ series) http://www.esrl.noaa.gov/psd/data/gridded/data.mlost.html (+ fields)
UDELv3.01	http://climate.geog.udel.edu/~climate/html_pages/download.html http://www.esrl.noaa.gov/psd/data/gridded/data.UDel_AirT_Precip.html (+)
AMIP20C	http://portal.nersc.gov/project/20C_Reanalysis (+)

[a] (+) shows the source used for the Figures and Tables.

Table S2. Temporal and spatial comparison of global TL_{2m} anomalies (90°N-60°S) from 20CR, station-temperature estimates and AMIP20C AGCM simulation[a].

	Temporal Correlation Annual	*Temporal Correlation Monthly High Pass*	*Pattern correlation (area mean removed)*	*Percentage of Land area where local trend is larger than 20CR*	*Global average Trend (change in °C per 50 years)*
1901-2010					
CRUTEM3	0.91	0.76	0.69 (0.23)	60%	0.58
CRUTEM4	0.90	0.77	0.74 (0.31)	62%	0.62
CRU_TS3.10*	0.90	0.81	0.72 (0.33)	47%	0.42
GISTEMP 250 km smoothing*	0.88	0.78	0.68 (0.18)	61%	0.61
JMATEMP*	0.89	0.74	0.67 (0.29)	63%	0.67
MLOSTv3.5.2*	0.92	0.81	0.78 (0.41)	63%	0.55
UDELv3.01*	0.84	0.81	0.68 (0.26)	37%	0.34
GISTEMP 1200 km smoothing	0.88	0.81	0.69 (0.17)	56%	0.53
AMIP20C	0.89	0.35	0.74 (0.32)	48%	0.45
1952-2010[b]					
CRUTEM3	0.95	0.84	0.79 (0.38)	70%	0.94
CRUTEM4	0.95	0.83	0.81 (0.42)	73%	1.0
CRU_TS3.10*	0.96	0.86	0.77 (0.37)	69%	0.96
GISTEMP 250 km smoothing*	0.96	0.85	0.78 (0.32)	74%	1.0
JMATEMP*	0.95	0.82	0.75 (0.36)	67%	0.98
MLOSTv3.5.2*	0.96	0.86	0.80 (0.37)	74%	0.96
UDELv3.01*	0.96	0.87	0.70 (0.21)	62%	0.90
GISTEMP 1200 km smoothing	0.96	0.85	0.80 (0.41)	77%	1.0
AMIP20C	0.89	0.36	0.73 (0.20)	53%	0.65

[a]*Temporal Correlation Annual* shows the Pearson correlation coefficient between the 20CR and the indicated dataset. *Temporal Correlation Monthly High Pass* shows the Pearson correlation coefficient between the 20CR and the indicated dataset after a 7-year running mean has been removed from each series. *Pattern Correlation* shows the area-weighted pattern correlation between the 20CR and indicated trend fields. The pattern correlation with the global land area-mean removed is shown in parentheses. The *Percentage of land* is the areal coverage of station-

204 temperature or simulated local temperature trends that are larger than 20CR trends. *Trend* is the
205 globally-averaged linear trend for each data set. The 20CR land-average trend is 0.45 °C/50
206 years using 1901-2010 and 0.67 °C/50 years using 1952-2010.
207 [b]Note that the year 1952 marks the first year after which the coefficients of the sampling and
208 modeling uncertainty parameterization, "covariance inflation", remain constant [Auxiliary
209 Material Section 2; Compo et al. 2011].
210

Table S3. Annually-averaged land temperature anomalies (60°N-60°S) from 20CR temporally compared with station-temperature estimates and AMIP20C.

	Temporal Correlation Annual [all P values <0.004]	*Mean Square Difference with 20CR (MSD, °C^2)*	*Expected Mean Square Difference with 20CR (°C^2) [P value for ratio with MSD]*
1901-2010			
CRUTEM3	0.91	0.0251	0.0103 [0.018]
CRUTEM4	0.91	0.0282	0.0105 [0.010]
CRU_TS3.10	0.91	0.0247	
GISTEMP 250 km smoothing	0.89	0.0356	
JMATEMP	0.89	0.0316	
MLOST	0.91	0.0432	0.015 [0.010]
UDEL	0.86	0.0301	
GISTEMP 1200 km smoothing	0.89	0.0299	
AMIP20C	0.88	0.0262	
1952-2010[a]			
CRUTEM3	0.95	0.0157	0.0028 [0.002]
CRUTEM4	0.95	0.0183	0.0030 [0.003]
CRU_TS3.10	0.96	0.0228	
GISTEMP 250 km smoothing	0.95	0.0257	
JMATEMP	0.94	0.0183	
MLOST	0.94	0.0277	0.0058 [0.027]
UDEL	0.96	0.0169	
GISTEMP 1200 km smoothing	0.95	0.0243	
AMIP20C	0.89	0.0190	

[a]Note that the year 1952 marks the first year after which the coefficients of the sampling and modeling uncertainty parameterization, "covariance inflation", remain constant [Auxiliary Material Section 2; Compo et al. 2011].

6. Auxiliary References

Anderson, J.L., and S.L. Anderson (1999), A Monte Carlo implementation of the nonlinear filtering problem to produce ensemble assimilations and forecasts, *Mon. Weather Rev.*, 127: 2741–2758, doi: 10.1175/1520-0493(1999)127<2741:AMCIOT>2.0.CO;2.

Ek, M. B., K. E. Mitchell, Y. Lin, E. Rogers, P. Grunmann, V. Koren, G. Gayno, and J. D. Tarpley (2003), Implementation of Noah land surface model advances in the National Centers for Environmental Prediction operational mesoscale Eta model, *J. Geophys. Res.*, 108, 8851, doi:10.1029/2002JD003296, D22.

Hamill, T.M., J.S. Whitaker, and C. Snyder (2001), Distance-dependent filtering of background error covariance estimates in an ensemble Kalman filter, *Mon. Weather Rev.* 129, 2776–2790, doi:10.1175/1520-0493(2001)129<2776:DDFOBE>2.0.CO;2.

Houtekamer, P.L., and H.L. Mitchell (2001), A sequential Ensemble Kalman Filter for atmospheric data assimilation, *Mon. Weather Rev.*, 129, 123–137, doi: 10.1175/1520-0493(1998)126<0796:DAUAEK>2.0.CO;2

Juang, H-M. (2005), Discrete generalized hybrid vertical coordinates by a mass, energy and angular momentum conserving vertical finite-differencing scheme. NCEP Office Note 445: pp 3. [Available online at: http://www.emc.ncep.noaa.gov/officenotes/FullTOC.html#2000].

Kalnay, E. (2003), *Atmospheric modeling, data assimilation, and predictability*. Cambridge University Press, Cambridge, UK, 364 pp.

M. Kanamitsu, J.C. Alpert, K.A. Campana, P.M. Caplan, D.G. Deaven, M. Iredell, B. Katz, H.-L. Pan, J. Sela, and G.H. White (1991), Recent changes implemented into the Global Forecast System at NMC. *Weather Forecasting*, **6**, 425–435, doi: 10.1175/1520-0434(1991)006<0425:RCIITG>2.0.CO;2.

McCormack, J.P., S.D. Eckermann, D.E. Siskind, and T. McGee (2006), CHEM2D-OPP: A new linearized gas-phase ozone photochemistry parameterization for high-altitude NWP and climate models, *Atmos. Chem. Phys.*, **6**, 4943-4972, doi: 10.5194/acpd-6-6627-2006.

Moorthi, S., Pan, H.-L., Caplan, P. (2001), Changes to the 2001 NCEP operational MRF/AVN global analysis/forecast system. Technical Procedures Bulletin 484, NOAA, NWS: Silver Spring, MD. Available from http://www.nws.noaa.gov/om/tpb/484.htm.

Saha, S., S. Nadiga, C. Thiaw, J. Wang, W. Wang, Q. Zhang, H. M. Van den Dool, H.-L. Pan, S. Moorthi, D. Behringer, D. Stokes, M. Peña, S. Lord, G. White, W. Ebisuzaki, P. Peng, and P. Xie (2006), The NCEP Climate Forecast System. *J. Clim.*, **19**, 3483–3517, doi: dx.doi.org/10.1175/JCLI3812.1.